Full-length article:

Imaging of Diluted Turbulent Ethylene Flames Stabilised on a Jet in Hot Coflow (JHC) Burner

Shortened running title:

Ethylene Flames in JHC Burner

Paul R. Medwell *, Peter A. M. Kalt and Bassam B. Dally

School of Mechanical Engineering, The University of Adelaide, S.A. 5005 Australia

Abstract

The spatial distribution of the hydroxyl radical (OH), formaldehyde (H_2CO) and temperature imaged by laser diagnostic techniques are presented using the Jet in Hot Coflow (JHC) burner. The measurements are of turbulent nonpremixed ethylene jet flames, either undiluted, or diluted with hydrogen (H_2), air, or nitrogen (N_2). The fuel jet issues into a hot and highly diluted coflow, at two O_2 levels and a fixed temperature of 1100K. These conditions emulate those of Moderate or Intense Low Oxygen Dilution (MILD) combustion. Ethylene is an important species in the oxidation of higher-order hydrocarbon fuels and in the formation of soot. Under the influence of the hot and diluted coflow soot is seen to be suppressed. At downstream locations surrounding air is entrained which results in increases in reaction rates and a spatial mismatch between the OH and H_2CO surfaces. In the very low O_2 coflow, a faint outline of the reaction zone is seen to extend to the jet exit plane, whereas at a higher coflow O_2 level the flames visually appear lifted. In the flames which appear lifted, a continuous OH surface is identified which extends to the jet exit. At the "lift-off" height a transition from weak to strong OH is observed, analogous to a lifted flame. H_2CO is also seen upstream of the transition point, **providing further evidence of** the occurrence of pre-ignition reactions in the apparent lifted region of these flames. **The unique characteristics of these particular cases has lead to the term *transitional* flame.**

Key words: JHC burner, MILD, Ethylene, OH, Formaldehyde, Rayleigh

* Corresponding Author. Tel: +61 8 8303 3157; Fax: +61 8 8303 4367
Email addresses: paul.medwell@adelaide.edu.au (Paul R. Medwell), pkalt@mecheng.adelaide.edu.au (Peter A. M. Kalt), bassam.dally@adelaide.edu.au (Bassam B. Dally).

1 Introduction

Heat and exhaust gas recirculation in combustors is an innovative approach to create a distributed reaction zone, reduce pollutant emissions and increase the net radiation flux, and with it thermal efficiency. It is now well established that a mixture of reactants diluted with combustion products, at a temperature above auto-ignition, can achieve the desired outcome of reduced pollutant emissions and enhanced thermal efficiency. The application of these principles to practical systems has taken different routes and different names used to describe the process. Some relied on a descriptive form of the resulting combustion process, i.e. Flameless Oxidation [1] and others described the features of the reactants streams, i.e. High Temperature Air Combustion. The term used in this paper is Moderate or Intense Low oxygen Dilution (MILD) combustion [2].

The MILD combustion technology has been successfully applied in several industries [3], and has the potential for introduction into numerous other applications [2]. To date however, implementation has been impeded by a lack of fundamental understanding of the establishment and detailed structure of this combustion regime. Few fundamental studies have been performed to look at the detailed structure of this regime (e.g. [2, 4–6]).

Dally et al. [4, 7] reported on the structure of hydrocarbon nonpremixed laminar and turbulent flames stabilised on a jet in a heated and diluted coflow. They used single-point Raman-Rayleigh-LIF diagnostic techniques to simultaneously measure temperature, major and minor species at different locations in these flames. They found that major changes in the flame structure occur when reducing the oxygen concentration and that, at higher jet Reynolds number and low oxygen con-

centration, oxygen leakage from the surroundings may cause local extinction of the flame. Medwell et al. [6] continued this work by simultaneous imaging of OH, H_2CO and temperature in the same burner finding evidence of partial premixing in these flames, and localised extinction in the presence of surrounding air.

The current project aims to examine the structure of the reaction zone of a jet in a heated and diluted coflow using planar laser imaging techniques. Temperature, the hydroxyl radical and formaldehyde are measured instantaneously and simultaneously at different parts of the flames. The hydroxyl radical (OH) is used as a flame marker while the formaldehyde (H_2CO) intermediate species is predominant at low temperatures typical of those found in MILD combustion. The product of $[OH]$ and $[H_2CO]$ has also been suggested as an indicator of the formyl (HCO) radical, which is closely related to the heat release rate [8].

In this paper we report on the combination of the three scalars in turbulent non-premixed diluted ethylene (C_2H_4) flames stabilised on a jet issuing into a heated and diluted coflow. The jet in hot coflow burner emulates MILD combustion under controlled conditions. Comparisons are made between different fuel compositions (ethylene undiluted, or diluted with hydrogen, air, or nitrogen) at a fixed jet Reynolds number and two coflow oxygen levels. Measurements are taken at two downstream locations. The burner used in this work facilitates the additional study of the effects of the entrainment of surrounding air on the flame structure at downstream locations.

Previous experiments have concentrated on methane fuel [4–7] due to its relatively simple chemistry. In order to bridge the gap to practical fuels, there is a need to investigate more complex hydrocarbons. Ethylene is an important intermediate in the oxidation of higher-order hydrocarbons, therefore making it suitable to examine

the effects of such fuels [9]. It is also an important species in the production of precursors leading to soot formation [10]. Mixing ethylene with inert as well as air and hydrogen have been used in the past to reduce soot. **The addition of hydrogen has practical implications for the potential use of hydrogen as a supplemental fuel additive. Air and nitrogen dilution enables the comparison of kinetic effects of partial premixing compared with inert dilution.** To the authors' knowledge, **these dilution effects of the primary fuel (i.e. ethylene) by other gases** has not previously been investigated in a hot and diluted coflow. As MILD combustion relies on effective mixing with inert and oxygen understanding the effect of each diluent in isolation aims to advance our understanding of this fuel.

2 Experimental Setup

The MILD combustion burner used in this study is the jet in hot coflow (JHC) burner used previously [6], and shown in Figure 1. It consists of a central insulated fuel jet (⌀4.6mm) within an annular coflow (⌀82mm) of hot exhaust products from a secondary burner mounted upstream of the jet exit plane. The fuel jet is more than 100 diameters in length to ensure fully developed pipe flow. The outer annulus is insulated with a fibrous blanket to minimise heat losses to the surrounds. The influences of the coflow remain ∼100mm downstream of the jet exit plane, beyond this the surrounding air begins to mix with the jet and coflow. The surrounding air entrainment facilitates the additional study of these effects on the reaction zone [6].

The O_2 level of the coflow is controlled by the constant flowrate secondary porous burner. The ratio of the coflow air/nitrogen was varied to give excess O_2 levels of 3% or 9% (volumetric), while the coflow temperature and exit velocity was kept constant at 1100K and 2.3m/s. Based on the annulus diameter the coflow Reynolds

number is $\sim$1400.

The fuel used in the jet is ethylene (>99% C_2H_4), either undiluted, or diluted with hydrogen (H_2), air or nitrogen (N_2). Table 1 shows the compositions and volumetric ratios of the jet flow. Addition of H_2 at this mixing ratio (1:1) has often been used in hydrocarbon flames to reduce soot interference [11], and is consistent with previous measurements in this burner [4, 6]. Similarly, air dilution (at 1:3 fuel/air) also cleans flames from soot [9] whilst not significantly altering the flame structure [12]. Nitrogen added at the same ratio subsequently allows the effects of inert dilution to be considered independently. **Any differences between the air and nitrogen diluted cases are directly attributable to the kinetic effects of O_2 in the fuel stream**. Also shown in Table 1 is the stoichiometric mixture fraction for both coflow O_2 levels and the mean jet exit velocity for a jet Reynolds number of 10,000 based on jet inner diameter.

Laser induced fluorescence (LIF) is used to image OH and H_2CO, and temperature is inferred from Rayleigh scattering measurements. Each species is probed with a separate laser system. Excitation of OH is at 283.222nm $(A - X\ (1,0)\ Q_1(7))$, and H_2CO via $A - X\ (2_0^1 4_0^1)\ ^pQ_{21}(5)$ at 340.836nm. The two LIF laser beams were produced from the frequency doubled output of dye lasers (Nd:YAG pumped at 532nm). The output power of the dye lasers was $\sim$2mJ/pulse for OH and $\sim$10mJ/pulse for H_2CO, with measured linewidths of 0.5cm^{-1} and 0.26cm^{-1} for OH and H_2CO, respectively. The source for the Rayleigh scatter was a $\sim$160mJ/pulse 532nm beam from a Nd:YAG laser. Detailed description of the LIF excitation schemes has previously been presented [6].

The experimental layout is shown in Figure 2. The three laser wavelengths are formed into overlapping co-planar laser sheets. The laser sheets pass through a

laminar slot burner (for reference purposes) in the same field of view as the JHC burner. The laser pulses are fired sequentially to reduce interferences on the other systems, with the entire sequence occurring in 300ns to ensure the flow field is frozen in time. Each species is detected normal to the laser sheet with a gated intensified CCD (ICCD) camera. To accommodate three separate cameras, a dichroic mirror is used between the OH and Rayleigh cameras. The dichroic reflectance is greater than 80% in the range 270–340nm, therefore acting as a broadband filter for the OH camera. The H_2CO and Rayleigh cameras were each fitted with long wave pass optical filters, GG-385 and GG-495 respectively. To minimise elastic scatter from particulate matter, gases were filtered and measurement locations chosen which were free of visible soot. The Rayleigh and H_2CO cameras were both used with $f_{\#}1.2$ lenses, and OH with a $f_{\#}4.5$ lens. The in-plane resolution of all three ICCD cameras is 160µm, after spatial matching. The light sheet thicknesses are estimated to be slightly larger than this, but of a similar order based on burns from photosensitive paper. The laser sheet heights were all $\sim$12mm, of which the central 8mm portion is presented herein. Further description of the experimental layout has been outlined in a previous publication by the authors [6].

3 Data Analysis

The images from the three ICCDs are spatially matched. Over the entire image the worst case mismatch is never more than 2 pixels (320µm), and after cropping the matching process gives sub-pixel accuracy. Each image is corrected for dark-charge, background and detector attenuation. All images are corrected for laser power and profile variations shot-to-shot based on the signal from the laminar slot burner. Based on the measurements from a flat-flame burner, the laser power shot-

to-shot corrections result in intershot variations of $\lesssim$5% for the OH and temperature. H_2CO shot-to-shot variations could not be accurately determined, but are expected to be of a similar order to the others. Approximately 400 images are recorded at each flame location and condition.

The temperature and composition change quite considerably both throughout the measurement volume and with different flame conditions. To account for these effects, consideration is given to the ground-state Boltzmann population distribution and collisional quenching effects. The specific correction procedures for the data is described in-depth in a previous publication by the authors [6]. One minor alteration over the previously reported Rayleigh to temperature conversion was required as some of the flames in the present work appear lifted, such that H_2CO is now included to assist in the determination of the jet/coflow boundary.

The signal to noise (SNR) of the instantaneous corrected images is typically better than 40:1 for OH, 10:1 for Rayleigh and 5:1 for H_2CO, although this value increases dramatically for H_2CO depending on the fuel composition.

Although Stokes-shifted Raman scatter from C_2H_4 coincides with the OH-LIF detection wavelength, because the LIF signal is much stronger this doesn't pose a major problem, and is only barely noticeable for the undiluted C_2H_4 flame.

It is noted that the H_2CO signal suffers only minor encroachment of vibrational Stokes-shifted Raman scatter from H_2 passing the detection filter. This interference is restricted to radial locations close to the centreline and has little effect near the flame location. **Interference from polycyclic aromatic hydrocarbons (PAH) can present a problem in H_2CO-LIF measurements. The selected excitation scheme has been reported as having lower broadband interference**

than other H_2CO schemes [13]. To confirm that PAH interference does not affect the findings, excitation wavelength scanning (in conjunction with a calibrated wavemeter) confirmed the locations of spectral peaks corresponding to H_2CO. Furthermore, for different flame conditions the trends in H_2CO-LIF agree with trends predicted by laminar flame calculations, and not with the trends of increased soot formation. While these observations do not provide categorical evidence, we are confident that PAH interference on the H_2CO-LIF signal does not significantly affect the results. Despite these issues, the H_2CO-LIF is sufficient to obtain reasonable understanding of the parameters that control its concentration and spatial distribution.

The images appearing in this paper have not been enhanced by image smoothing to reduce inter-pixel noise.

4 Results

4.1 Visual Observations

Figure 3 shows photographs of the flames presented in this paper and the two measurement locations, centred at 35mm and 125mm above the jet exit plane. These measurement locations were chosen to represent two oxidant regimes. At the 35mm location, the oxidant stream is that of the coflow (with a specified O_2 level) while at the 125mm location air from the surrounds is entrained with the coflow stream resulting in a different oxidant composition than at the 35mm location. It is clearly apparent that for all flames a reduction in O_2 level has lead to a decrease in flame luminosity. This change in luminosity is attributed to the reduction in temperature and the different intermediates formed in each of the flames. Furthermore, it should

be noted that due to the vast differences in the luminosity of the flames, the exposure times have been varied while all other camera parameters held constant.

For either coflow O_2 level, where the coflow influences the jet flame ($\lesssim$100mm) soot is not apparent. Generally ethylene fuel has a tendency to produce large amounts soot, especially with an elevated coflow temperature, but under the current low O_2 coflow conditions soot is not observed. It is only at downstream locations where the surrounding air begins to penetrate the coflow that soot appears. The presence of soot for some of the 9% O_2 flames (C_2H_4 and C_2H_4/H_2) at 125mm downstream could lead to interferences with the Rayleigh and LIF measurements, and so data collection at 125mm is limited to the 3% O_2 case only.

Except for the C_2H_4/H_2 flame, all of the 9% O_2 coflow flames visually appear lifted by $\sim$30mm. For all 3% O_2 flames a very faint outline may be seen to extend to the jet exit plane, although this **may be** difficult to see in the photographs. The lack of luminosity under MILD combustion conditions almost gives the 3% O_2 flames the misleading appearance that they are lifted – they are attached however. Based on the photographs, what appears to be the lift-off heights for the 9% O_2 flames are presented in Table 2. **Later in this paper, it will be shown that there is some dispute as to whether or not these flames are in fact attached. Rather than referring to them as lifted, these flames will be described as having a transition in the reaction zone.**

The photographs and data presented in Figure 3 and Table 2 are for a jet Reynolds number of 10,000 (based on jet inner diameter). By altering the jet velocity, the apparent lift-off heights have been determined at other jet Reynolds numbers as well, with the results shown in Figure 4. From this figure it is noted that increasing the jet velocity leads to a *reduction* in apparent lift-off height, especially between

jet Reynolds numbers of 5000 and 10,000, beyond which the effects are less pronounced. This trend is contradictory to the expected trends for lifted flames under conventional conditions. It is noteworthy that under the heated coflow conditions the Re_{jet}=5000 case borders a transition to turbulence conditions. Increasing the Reynolds number beyond 10,000 shows a much lower decrease in lift-off height.

4.2 Instantaneous Images at Axial Location 35mm downstream

Figure 5 shows typical instantaneous image triplets of OH, H_2CO and temperature at the 35mm downstream location, for each of the fuel compositions at two coflow O_2 levels. The corresponding size of each image is 8×30mm. The jet centreline is indicated by the vertical dashed line. The data presented is for a jet Reynolds number of 10,000 for all cases. Data at different Reynolds numbers shows the same trends seen here and are not presented in this paper.

The temperature images show a uniform temperature distribution in the coflow stream. From the OH images in Figure 5 it is clear that there exists vast differences in the relative OH number density for the various flames. The colour scaling for Figure 5 has been chosen to overemphasise the low OH levels, resulting in much of the OH to appear saturated. Very small quantities of OH can be seen in the coflow and are equivalent to equilibrium levels. The spatial location of H_2CO on the fuel-rich side, in relation to OH, reinforces that H_2CO is a first-step intermediate [14] formed as a product of fuel decomposition [15]. The H_2CO levels differ from one fuel composition to another and are also influenced by the O_2 level in the coflow.

The broad radial distribution of the H_2CO which is seen in the instantaneous images of Figure 5 is also noted in laminar flame calculations. Figure 6 shows

the calculated H_2CO number density using the OPPDIF code of the Chemkin package with GRI-Mech version 3.0 mechanism. Since the coflow oxidant stream consists of combustion products (H_2O and CO_2), the standard definition of mixture fraction is not appropriately defined for calculations based on the mass fraction of H & C (hydrogen & carbon) atoms. To compensate for this, a normalised mixture fraction (ξ^*) is defined based on the mixture fraction found from the calculations (ξ) such that $\xi^* = (\xi - \xi_{oxi}) / (\xi_{fuel} - \xi_{oxi})$; where ξ_{fuel} & ξ_{oxi} refer to the standard definition of mixture fraction at the fuel and oxidant stream boundaries, respectively. Figure 6 provides clear evidence that the broad radial distribution of H_2CO is indeed genuine, and not due to PAH interference.

As already highlighted, all of the 3% O_2 coflow flames were visually identified as being attached. This is confirmed in the OH images of Figure 5 where a continuous OH surface is seen in each of the 3% O_2 images. The images show a substantial suppression of OH levels in the low O_2 coflow, consistent with previous work (e.g. [6, 16]) and is directly related to the reduced temperature of the reaction zone. For most of the 3% O_2 flames the temperature peak across the reaction zone is barely discernable, although a definite OH layer is measured. It is noted that a temperature increase is seen in the air diluted flame in relation to the other fuel compositions for a 3% O_2 coflow. **This observation is supported by simple laminar flame calculations using the OPPDIF code of the Chemkin package (GRI-Mech 3.0 mechanism), which predict a peak temperature increase of $\sim$150K relative to the undiluted jet.**

At the 9% O_2 coflow the OH images reveal significant differences to the 3% case, most notably the observation that these flames initially appear lifted. The identified lift-off heights from visual observations are at around the same downstream loca-

tion as the measurement location. Fluctuations in the apparent lift-off height results in some of the 9% O_2 instantaneous images including strong OH whilst others do not. Figures 5b, 5f & 5h typify the characteristics seen at the base of lifted flames. Closer inspection of the 9% images reveals some interesting observations. Except for the H_2 diluted flame (which is attached), the 9% images presented in Figure 5 have been chosen to show what seems to be the bottom of a lifted flame. Beneath the strong OH, in each of the lifted images a weak tail is seen towards the bottom. **This OH tail is seen to persist as the Reynolds number is increased.**

Figure 7 presents a further selection of images from the flames that appear lifted. The lack of strong OH in these images indicates that these instances are below an instantaneous apparent lift-off height, nevertheless, a discernable OH surface is seen. As the apparent lift-off height of the undiluted flame is less than the other flames, at the measurement location no images were identified where there was no strong OH in the image. The lower parts of image Figure 7a show the same features as the other flames in Figure 7 however.

The presence of H_2CO in conjunction with the OH in the images tends to suggest that there is in fact a pre-ignition reaction taking place below what appears to be the lift-off height. Formation of H_2CO early in the ignition process has been noted previously in similar conditions [17]. Coupled with the OH observations, formation of H_2CO casts further doubt over the visual observation of these flames being lifted. The apparent lift-off height corresponds to a transition of weak to strong OH levels. As such, rather than identifying a “lift-off” height it is more appropriate to refer to this as a transition point. The general observations relating to this transition point seem to be analogous to conventional lifted flames.

It is interesting to note that the H_2CO levels are similar at each axial location

whether there is strong OH or not. Modelling efforts of Gkagkas & Lindstedt [17] suggest that the H_2CO concentrations reach a maximum just before the flame front – such an increase is not seen in the images presented here. Moreover, the H_2CO distribution shows a relief along the jet centreline and exists on the fuel-rich side, whereas Gkagkas & Lindstedt [17] present a continuation of the H_2CO to the centreline. For each of the fuel compositions, the H_2CO levels in the 3% O_2 coflow are less than for the 9% O_2 case. The H_2 diluted flame has significantly lower H_2CO levels than the other flames, leading to the very weak H_2CO-LIF signal.

The general expectation that OH increases is associated with an increase in temperature are not necessarily seen in the images presented. Several instances are noted where there is strong OH present yet the temperature shows no increase. This observation is frequently noted in the 3% O_2 coflow, but is also seen at the 9% O_2 coflow, and is consistent with previous work in a similar high temperature oxidant stream environment [18].

4.3 Mean and RMS quantities at Axial Location 35mm downstream

Table 3 shows the averaged peak OH values in each of the images for a particular flame, also included is the standard deviation (as a percentage). In determining the peak value in each of the images, only the central portion of the image is included to avoid over-corrected values towards the edges of the images where the low laser power makes sheet corrections less reliable.

As expected, the OH number density at the 3% O_2 coflow is lower than the 9% case. For the 3% O_2 coflow, the mean peak OH number density seems quite independent on the fuel composition, although a $\sim$3 fold increase is found in the

C_2H_4/H_2 flame. The increase of OH in this flame, which is consistent with laminar flame calculations, is not a product of increased temperature but is attributed to the presence of H_2.

At the 9% O_2 level the apparent lifted nature of these flames limits making comparisons between these flames and are only included to highlight this very issue. As already highlighted, and seen in the images of Figures 5 & 7, at the 35mm measurement location the base of strong OH is intermittently captured in the images. This intermittency leads to the very high standard deviation for the air and nitrogen diluted flames, and also skews the mean OH number density. The undiluted flame also appears lifted, but slightly less than the other two, such that the base of strong OH is always captured, as indicated by the much lower standard deviation and the higher mean OH number density.

The averaged H_2CO peak values (and standard deviation) from the instantaneous images are also presented in Table 3. As with the OH peak values, only the central portion of the images is included. As expected due to oxygenation of the fuel [19], and consistent with the instantaneous images of Figure 5, at 3% O_2 with air dilution the H_2CO levels are highest. At the 9% O_2 coflow the undiluted flame mean H_2CO levels are higher than the air diluted flame. This difference is not well understood and is likely to be an artefact of the apparent lift-off and the pre-ignition chemistry of the different fuels. The intermittency of the lift-off height observed in the OH number density standard deviations is not reflected in the H_2CO standard deviation for the lifted 9% flames. The consistency in the H_2CO levels was also noted in the instantaneous images of Figure 5.

Figure 8 shows the mean and RMS radial profiles of OH, H_2CO and temperature for both 3% and 9% O_2 for the various fuel compositions, and at an axial location

35mm above the jet exit plane. As most of the 9% O_2 flames appear lifted, direct comparison between the two O_2 levels is less meaningful. For the H_2 diluted flame however, it is clear from Figure 8 that reducing the O_2 levels leads to a substantial decrease of OH as already seen in the instantaneous images. It is also noted that minor equilibrium OH levels in the coflow stream are observed at both coflow conditions. At 3% O_2, except for the hydrogen diluted flame, the mean OH profiles virtually overlap. The much higher levels of OH for the H_2 diluted flame was also reflected in Table 3. The trends seen in the 9% O_2 flames are in agreement with the values in Table 3.

In the undiluted ethylene flames a very slight increase in OH-LIF signal is seen towards the jet centreline. As outlined in §3, this effect is attributed to Raman interferences from the C_2H_4, and does not influence any of the current findings as it is readily disregarded based on the spatial location relative to the reaction zone. From both the mean plots and the instantaneous images in Figure 5 the extraneous OH-LIF signal along the centreline is seen to drop to zero before it increases through the reaction zone. This is further evidence of the interference being due to C_2H_4. Due to dilution of C_2H_4 for the other fuel composition this interference is not seen.

4.4 Instantaneous Images at Axial Location 125mm downstream

At the 125mm downstream location it is visibly evident that the flames are perceptibly different in structure, as seen in Figure 3. At this location the surrounding air is able to mix with the hot coflow. As seen in the photographs, soot becomes apparent at this location for the 9% O_2 coflow flames, limiting laser diagnostic measurements of these scalars to the 3% case only. The presence of soot particulate could potentially interfere with the Rayleigh scatter.

Figure 9 shows the mean and RMS radial profiles of OH, H_2CO and temperature for a 3% O_2 coflow for the various fuel compositions, and at an axial location 125mm above the jet exit plane. In comparison to the equivalent plot at 35mm downstream (Figure 8) it is apparent that the radial distribution becomes broader and peaks at a wider radial location, due to the spreading of the jet.

Figure 10 shows typical images for the various 3% O_2 flames at the 125mm axial location. At the downstream location, the entrainment of additional oxygen from the surrounds into the coflow results in increased reaction rates. This in turn leads to increases in the OH and temperature at the downstream locations compared to the 35mm position. Of particular note in these images is the mismatch between the OH and H_2CO surfaces. Although the OH and H_2CO demarcate the fuel lean and rich sides of the reaction zone, respectively, the spatial separation between the two is extraordinarily large – for the nitrogen diluted image presented in Figure 10d the separation is $\sim$5mm. This separation is not due to experimental error in the matching of the images since correlation of a target image before and after the runs does not exhibit the spatial variation seen in the images of the species in the flame. Furthermore, a temperature increase is noted to follow the respective borders of the void between the OH and the H_2CO. **The separation is likely to be due to the consumption of the H_2CO well in advance of the reaction zone due to the high temperature in this region, as has been noted previously [17]**.

Table 4 presents the averaged peak OH and H_2CO values for each flame, also included is the standard deviation (as a percentage). As was also seen in Table 3, at the downstream location the OH number density is relatively constant for the different fuel compositions. A slight reduction in peak OH is noted for the N_2 diluted flame – which also has the highest standard deviation in the peak OH value. For the H_2CO, from Table 4 the air diluted flame is seen to have a peak value four times

higher than the other fuel compositions, as expected, and consistent with the 35mm data.

5 Discussion

5.1 Effect of coflow composition

The most noticeable difference between the two coflow oxygen levels is noted in the apparent lift-off phenomenon observed. At the higher (9%) O_2 level, the flames visually appear lifted, but the OH tends to indicate a continuous reaction extending to the jet exit.

In this study we ascertain the lift-off height based on visual observation and long-exposure photography rather than an arbitrary choice of chemiluminescence, as has been used in other previous work (e.g. [24]) or a defined OH mass fraction (e.g. [25, 26]). The different approach is not expected to lead to the variations noted however. Moreover, during the experiments as the jet flowrate was increased the apparent lift-off height was visually seen to decrease. It is worth mentioning that hysteresis effects which occur in flames without a hot coflow [22] are not expected to lead to the differences in the apparent lift-off heights seen here because of the hot coflow. The coflow temperature is above auto-ignition and so this is believed to counteract any hysteresis effects.

Lift-off height is generally considered to be directly proportional to the jet exit velocity [22], whereas increasing the jet velocity (jet Reynolds number) for these flames is seen to decrease the lift-off height (Figure 4). The different trend in transition height with jet velocity is likely due to an increase in mixing near the jet exit.

A similar observation has been previously noted in a MILD combustion furnace. Dally et al. [27] reported that an increase in jet velocity helped to stabilise their flames closer to the jet exit. This trend highlights the differences in the stabilisation mechanisms of these flames as compared with conventional lifted flames. The likely cause of such trend may be related to the increase in mixing at the shear layer which shortens the ignition delay resulting in shorter lift-off height. Further investigation of this phenomenon is warranted.

The observation of the transition from weak to strong OH in the higher O_2 flames is analogous to a lifted flame. Such a transition is not seen in the lower O_2 flames however. The transition which occurs at the 9% O_2 level and not at 3% O_2 could be due to a shift in the stoichiometric mixture fraction towards the fuel rich side, where the interactions with the jet shear layer are higher. Another alternative may be that the *flame induced* strain rates are reduced because of the lower reaction rates.

It is noted that the OH number density below the transition point in the 9% O_2 flames is at similar levels to the attached 3% O_2 flames. For the 3% flames, the luminosity of the entire flame is very low, allowing us to distinguish the very faint outline of the reaction zone down to the jet exit plane. The more luminous flame brush of the 9% flames may mask such a reaction zone outline in the 9% flames. If it were possible to isolate the light from luminous brush perhaps a reaction zone outline may be able to be identified in the lower parts of the 9% flames as well.

In contrast to the present work, under similar vitiated conditions Gordon et al. [24] observed a linear dependence of lift-off height with jet velocity. Four significant differences are noted between the current work and that of Gordon et al. [24]; (1) different O_2 level in coflow, (2) different fuel and coflow composition, (3) different jet velocities and (4) different coflow velocity. It is important to recognise the

extreme sensitivity of the lift-off height with coflow temperature [26] and also the coflow velocity [21]. The clear trend of lift-off height with jet velocity for the various fuel dilutions suggests that the sensitivity of the lift-off height is not likely to be responsible for the trends seen in the current data. It is relevant to note that Gordon et al. [24] used the same burner design as Cabra et al. [25]. In the work of Cabra et al. the OH mass fraction results show a lifted flame, but the PDF reaction progress shows a reaction taking place well upstream of the main OH contours. Furthermore, a *very* faint OH outline is seen in Figure 3 of Cabra et al. [25]. The barely discernable OH tail seems to be consistent with the current results. The relative intensity of the weak OH in the tail and the much stronger OH downstream of the "lift-off" height is far more pronounced in Cabra et al.'s work as compared with the current data. This is expected to be due largely to the differences in the O_2 levels and potentially the coflow temperature as well.

The reason for the presence of the weak OH upstream of the transition point seen in the images does not seem to be due to the reverse flow observations made by Upatnieks et al. [28] or the existence of products further upstream by Tacke et al. [29]. The high temperatures of the coflow stream suggest that the characteristic S-shaped curve for ignition and extinction collapses into a monotonic function [16], consequently separate ignition and extinction events do not occur [30]. This seems to be a relevant observation regarding the detection of OH in what appears a non-reacting region. It is particularly important that despite the proposition of a monotonic function for extinction/ignition, a bimodality under MILD combustion conditions has been observed [27]. It is mooted that under MILD conditions perhaps the extinction/ignition phenomenon manifests itself as a weak/strong reaction. This transition leads to a bimodal behaviour, without explicit extinction/ignition occurring.

The intimation that there may be a reaction taking place upstream of the transition

height *does not* categorically conflict with the potential of a lifted flame. The reaction which is in discussion is not considered to be a fully fledged flame, rather some kind of pre-ignition reaction. Being a much less intense reaction, entrained mixing with the oxidant stream is capable of permeating through the "reaction" zone, leading to premixing at the transition height, thus resulting in the stronger OH levels after a certain downstream distance.

The role of the pre-ignition reaction taking place upstream of the transition height does not seem to significantly alter the remainder of the flame. Cabra et al. [25] showed that under similar heated and diluted coflow conditions conventional scaling arguments seemed to predict the lift-off height for their work, suggesting that the overall characteristics of the flame were not significantly varied from a standard flame. As Cabra et al. [25] noted, the different temperature of the coflow may alter the mechanisms relating to lift-off despite the similar global observations between the vitiated and conventional conditions. This is in relative agreement with our findings. We acknowledge that a reaction upstream of the transition height does not significantly effect the downstream reactions, but tends to suggest a different kinetic role in the stabilisation mechanism.

5.2 Effects of fuel composition

It is clear from the flame photographs of Figure 3 that changing the fuel composition alters the visual appearance of the flames. Differences between the flames are not as obvious in the OH concentrations seen in Table 3 and Figure 8. More significant differences are seen in the H_2CO concentration profiles of Figure 8.

When comparing the effect of fuel dilution, focus is placed on the 3% O_2 flames be-

cause these are all attached. The highest H_2CO levels are expected in the air diluted (partially premixed) flame over the nonpremixed flames. Partial premixing leads to at least five times H_2CO levels as in nonpremixed methane flames [19]. The effect of premixing is even more pronounced for ethylene, where small amounts of premixing (Φ=24) are reported to lead to a eight-fold increase in formaldehyde over the nonpremixed flame [9]. The equivalence ratio of the air diluted flame in the current study is $\Phi\approx$4.8, which is expected to have maximum H_2CO levels $\sim$15 times larger than the undiluted flame [9] – much greater than the increases seen in Figure 8. It is imperative to highlight that the peak H_2CO concentrations of McEnally & Pfefferle [9] are based on centreline data, at a much further downstream location and at laminar conditions. It has previously been shown that Reynolds number has a significant effect on H_2CO concentrations [6]. Nevertheless, the trends of H_2CO increase are consistent. Furthermore, even in an un-questionably attached flame under conventional conditions some O_2 penetrates to the jet centreline, resulting in some form of premixing even in attached flames [19]. The effect of oxygen permeating through the flame front zone is expected to be more pronounced as a result of the lower reaction rates at the low O_2 coflow conditions in our flames, enhanced by the thermal diffusion due to the hot coflow. The potential for oxygen leakage through the reaction zone in the low O_2 flames may lead to higher H_2CO levels in the undiluted flames as compared to an ideal nonpremixed flame, and so the effects of partial premixing may be reduced.

The dilution rate for the partially premixed (air diluted) and inert (nitrogen) diluted flames is the same. Any differences between the two are directly attributed to the effects of the additional oxygen, with only a slight change in stoichiometric mixture fraction. The OH concentrations and the general features of the images remain essentially constant for either diluent. Increases in the peak H_2CO and temperature

are noted with air dilution, while retaining the same features. Partial premixing of the flame therefore seems to increase reaction rates, but not significantly alter the inherent structure of the reaction zone. It is generally accepted that at this level of premixing the flame retains all the nonpremixed flame features, which seems to hold true in heated and diluted conditions as well.

Hydrogen dilution leads to the most noticeable variations in the measured species. Concentrations of OH increase markedly, while H_2CO levels drop dramatically. Addition of H_2 also gives rise to the 9% O_2 flames attaching, unlike any of the other cases. The addition of H_2 to the fuel is expected to lead to an attached flame as it is known that H_2 acts as an ignition promoter [17].

Small degrees of partial premixing increases soot volume fractions in ethylene flames, but for equivalence ratios below about $\sim$15 soot volume fractions subsequently decrease [9]. The equivalence ratio of the partially premixed flame in this paper is $\Phi \approx 4.8$, and so the premixing is expected to reduce levels of soot, as seen in Figure 3.

Increasing the stoichiometric mixture fraction (by means of fuel dilution) causes the location of the reaction zone to shift towards the shear layer, having an influence on the flame structure [31]. Moreover, shifting the stoichiometric mixture fraction closer to the fuel side can be linked to a decrease in soot formation [32]. The stoichiometric mixture fraction of the 9% flames is greater than the 3% flames, suggesting that if the stoichiometry shift was the only difference between the two O_2 cases the 9% flames would exhibit less soot – which does not appear to be the case. This suggests that the soot suppression by means of reducing the O_2 level is related to the chemical effects of the hot coflow and not the shift in stoichiometry.

The effects of the hot and diluted coflow on the levels of soot seem to extend be-

yond the region where the oxidant composition is controlled by the coflow. As a generalisation, soot does not appear until ∼200mm downstream of the jet exit. The coflow is known to persist only approximately 100mm downstream [6], and so, it seems that the initial conditions have a significant role on the intermediates that are formed, which in turn alter the downstream behaviour of the flames.

5.3 General observations

A triple flame consists of a lean and rich premixed flames surrounding a diffusion flame. Joedicke et al. [20] have presented images of lifted methane and methane/nitrogen flames suggesting evidence of a triple flame structure. Their flames consisted of a simple fuel jet issuing into a nominal coflow. The heated coflow used in our work seems to provide a fundamentally different environment to that of Joedicke et al. [20]. Comparison of our imaging to that of Joedicke et al. [20] reveals significant differences in the distribution of OH and H_2CO. The differences are particularly evident in the H_2CO images. Without a heated coflow, the H_2CO only appears around the base of the lifted flame [20], whereas with a heated coflow the H_2CO is seen to exist well below the lift-off height (Figure 7).

Imaging of OH alone is insufficient to identify a triple flame structure [21], but coupled with H_2CO it may be possible to infer a triple flame. In a triple flame the H_2CO should "wrap around" the OH, thereby creating two H_2CO peaks, each demarcating the fuel lean and rich branches. In general, our images do not show evidence of a triple flame structure existing in our flames. A few images show some signs of two H_2CO branches (Figure 11), but no H_2CO is present at what would be deemed the triple point. The cause of the H_2CO distribution seems far more likely to be due to vortical structures rather than a triple flame.

While we have no evidence of triple flames, and a significantly different H_2CO distribution, we cannot categorically confirm or deny the existence of a triple flame. The turbulent nature of our flames may lead to a compression of the triple flame such that its presence would be masked [22]. As reported by Joedicke et al. [20], and noted by Im & Chen [23], as turbulence levels increase the interaction of vortices with a triple flame cause the branches of a triple flame to collapse into an edge flame.

6 Conclusion

Simultaneous imaging measurements of the hydroxyl radical (OH), formaldehyde (H_2CO) and temperature of turbulent nonpremixed diluted ethylene flames in the Jet in Hot Coflow (JHC) burner have been presented. The heated and highly diluted coflow conditions (either 3% or 9% O_2, constant temperature of 1100K) provided by this burner emulate those of MILD combustion. Results have been presented at two coflow O_2 levels for a fixed jet Reynolds number of 10,000 and diluents of either hydrogen (H_2), air, or nitrogen (N_2).

Soot production of the notoriously sooty ethylene fuel is shown to be suppressed under the influence of the hot and diluted coflow. For either coflow O_2 level, where the coflow influences the jet flame, soot is not apparent. Even at downstream locations, where the surrounding air begins to penetrate the coflow, the effects of the hot and diluted coflow on the levels of soot seem to persist. It is only well beyond the extent of the coflow that soot is noticed. It appears that the initial conditions have a significant role on the formation of the precursors to soot, which in turn alter the downstream behaviour of the flames.

At the downstream measurement location, the entrainment of additional oxygen from the surrounds into the coflow results in increased reaction rates. This in turn leads to increases in the OH and temperature at the downstream locations compared to closer to the jet exit plane. Of particular note in the downstream measurements is a spatial mismatch between the OH and H_2CO surfaces. The separation is likely to be due to the consumption of the H_2CO well in advance of the reaction zone due to the high temperature in this region.

At the 3% O_2 coflow case a faint outline is visually seen to extend to the jet exit plane, whereas the higher 9% O_2 flames visually appear lifted. The apparent lift-off height decreases with an increase in jet velocity, contradictory to conventional trends. In the flames which appear lifted, a continuous OH surface can be identified which extends to the jet exit. Nevertheless, at the "lift-off" height a transition from weak to strong OH is observed, analogous to lifted flames. H_2CO is also seen upstream of the transition point. Although not a fully reacting flame, the presence of these intermediates indicates the occurrence of pre-ignition reactions upstream of the transition point of these flames.

The detection of flame species upstream of the transition height does not necessarily imply that the flames are or are not lifted. The reactions which occur in the "lifted" region are believed to be associated with pre-ignition reactions rather than a fully developed flame front. There may be some dispute over the terminology of this phenomenon. Given that conventionally lifted flames do not exhibit pre-ignition reactions in the same way, it does not seem justifiable to also refer to these flames as lifted. Describing these flames as having a transition in reaction zone structure seems a more accurate depiction. The measurements suggest that jet velocity plays an important role in promoting mixing to aid in the stabilisation of these flames. It is clearly apparent that

MILD combustion conditions provide a fundamentally different mechanism for flame stabilisation.

Acknowledgments

The authors would like to thank Dr Zeyad Alwahabi for his assistance with this project. The financial support of The University of Adelaide and the Australian Research Council is gratefully acknowledged.

References

[1] J. A. Wünning, J. G. Wünning, Flameless oxidation to reduce thermal NO-formation, Progress in Energy Combustion and Science 23 (1997) 81–94.

[2] A. Cavaliere, M. de Joannon, Mild combustion, Progress in Energy and Combustion Science 30 (2004) 329–366.

[3] J. G. Wünning, FLOX® — Flameless Combustion, Thermprocess Symposium 2003, WS Wärmeprozesstechnik GmbH, (2003).

[4] B. B. Dally, A. N. Karpetis, R. S. Barlow, Structure of turbulent non-premixed jet flames in a diluted hot coflow, Proceedings of the Combustion Institute, Volume 29 (2002) pp. 1147–1154.

[5] C. Ahn, F. Akamatsu, M. Katsuki, A. Kitajima, The influences of mixture composition and preheat temperature on combustion regime and flame structure of premixed turbulent flames, The Fourth Asia-Pacific Conference on Combustion, (2003) pp. 40–43.

[6] P. R. Medwell, P. A. M. Kalt, B. B. Dally, Simultaneous Imaging of OH, Formaldehyde and Temperature of Turbulent Nonpremixed Jet Flames in a Heated and Diluted Coflow, Combustion and Flame 148 (2007) 48–61.

[7] B. B. Dally, A. N. Karpetis, R. S. Barlow, Structure of Jet Laminar Non-premixed Flames under Diluted Hot Coflow Conditions, 2002 Australian Symposium on Combustion and The Seventh Australian Flame Days, Adelaide, Australia (2002).

[8] H. N. Najm, P. H. Paul, C. J. Mueller, P. S. Wyckoff, On the adequacy of certain experimental observables as measurements of flame burning rate, Combustion and Flame 113 (1998) 312–332.

[9] C. S. Mc Enally, L. D. Pfefferle, Experimental study of nonfuel hydrocarbons and soot in coflowing partially premixed ethylene/air flames, Combustion and

Flame 121 (2000) 575–592.

[10] C. J. Sun, C. J. Sung, H. Wang, C. K. Law, On the structure of nonsooting counterflow ethylene and acetylene diffusion flames, Combustion and Flame 107 (1996) 321–335.

[11] H. Guo, F. Liu, G. J. Smallwood, Ö. L. Gülder, Numerical study on the influence of hydrogen addition on soot formation in a laminar ethylene-air diffusion flame, Combustion and Flame 145 (2006) 324–338.

[12] S. H. Stårner, R. W. Bilger, R. W. Dibble, R. S. Barlow, Piloted diffusion flames of diluted methane near extinction: Detailed structure from laser measurements, Combustion Science and Technology 72 (1990) 255–269.

[13] P. H. Paul, H. N. Najm, Planar laser-induced fluorescence imaging of flame heat release rate, Proceedings of the Combustion Institute, Volume 27 (1998) pp. 43–50.

[14] R. Bombach, B. Käppeli, Simultaneous visualisation of transient species in flames by planar-laser-induced fluorescence using a single laser system, Applied Physics B 68 (1999) 251–255.

[15] K. Kohse-Höinghaus, J. B. Jeffries, Applied Combustion Diagnostics, Taylor & Francis (2002).

[16] T. Plessing, N. Peters, J. G. Wünning, Laseroptical investigation of highly preheated combustion with strong exhaust gas recirculation, Proceedings of the Combustion Institute, Volume 27 (1998) pp. 3197–3204.

[17] K. Gkagkas, R. P. Lindstedt, Transported PDF modelling with detailed chemistry of pre– and auto–ignition in CH_4/air mixtures, Proceedings of the Combustion Institute, Volume 31 (2007) pp. 1559-1566.

[18] R. L. Gordon, M. J. Dunn, A. R. Masri, R. W. Bilger, Joint Imaging of Rayleigh and LIF-OH at the Base of Lifted Flames Issuing in Vitiated Coflow, Fourth Australian Conference on Laser Diagnostics in Fluid Mechanics and

Combustion, The University of Adelaide, South Australia, Australia, (2005) pp. 45–48.

[19] C. S. McEnally, L. D. Pfefferle, Experimental Study of Nonfuel Hydrocarbon Concentrations in Coflowing Partially Premixed Methane/Air Flames, Combustion and Flame 118 (1999) 619–632.

[20] A. Joedicke, N. Peters, M. Mansour, The stabilization mechanism and structure of turbulent hydrocarbon lifted flames, Proceedings of the Combustion Institute, Volume 30 (2005) pp. 901–909.

[21] T. Plessing, P. Terhoeven, N. Peters, M. S. Mansour, An experimental and numerical study of a laminar triple flame, Combustion and Flame 115 (1998) 335–353.

[22] M. S. Mansour, Stability characteristics of lifted turbulent partially premixed jet flames, Combustion and Flame 133 (2003) 263–274.

[23] H. G. Im, J. H. Chen, Structure and propagation of triple flames in partially premixed hydrogen-air mixtures, Combustion and Flame 119 (1999) 436–454.

[24] R. L. Gordon, S. H. Stårner, A. R. Masri, R. W. Bilger, Further characterisation of lifted hydrogen and methane flames issuing into a vitiated coflow, 5^{th} Asia-Pacific Conference on Combustion, The University of Adelaide, Adelaide, Australia (2005) pp. 333–336.

[25] R. Cabra, T. Myhrvold, J. Y. Chen, R. W. Dibble, A. N. Karpetis, R. S. Barlow, Simultaneous laser Raman-Rayleigh-LIF measurements and numerical modelling results of a lifted turbulent H_2/N_2 jet flame in a vitiated coflow, Proceedings of the Combustion Institute, Volume 29 (2002) pp. 1881–1888.

[26] R. R. Cao, S. B. Pope, A. R. Masri, Turbulent lifted flames in a vitiated coflow investigated using joint PDF calculations, Combustion and Flame 142 (2005)

438–453.

[27] B. B. Dally, E. Riesmeier, N. Peters, Effect of fuel mixture on moderate and intense low oxygen dilution combustion, Combustion and Flame 137 (2004) 418–431.

[28] A. Upatnieks, J. F. Driscoll, S. L. Ceccio, Cinema particle imaging velocimetry time history of the propagation velocity of the base of a lifted turbulent jet flame, Proceedings of the Combustion Institute, Volume 29 (2002) pp. 1897–1903.

[29] M. M. Tacke, D. Geyer, E. P. Hassel, J. Janicka, A detailed investigation of the stabilization point of lifted turbulent diffusion flames, Proceedings of the Combustion Institute, Volume 27 (1998), pp. 1157–1165.

[30] I. B. Özdemir, N. Peters, Characteristics of the reaction zone in a combustor operating at MILD combustion, Experiments In Fluids 30 (2001) 683–695.

[31] J. B. Kelman, A. R. Masri, Quantitative technique for imaging mixture fraction, temperature, and the hydroxyl radical in turbulent diffusion flames, Applied Optics 36 (15) (1997) 3506–3514.

[32] J. Du, R. L. Axelbaum, The effect of flame structure on soot-particle inception in diffusion flames, Combustion and Flame 100 (1995) 367–375.

Fuel Composition	Volumetric ratio	f_{stoich} 3% O_2	f_{stoich} 9% O_2	U_{jet} [m/s]	Re_{jet} [–]
C_2H_4	–	0.010	0.029	17.5	10,000
C_2H_4/H_2	1:1	0.009	0.027	30.6	10,000
C_2H_4/Air	1:3	0.050	0.135	27.3	10,000
C_2H_4/N_2	1:3	0.039	0.108	27.3	10,000

Table 1
Fuel jet dilution ratios of ethylene (C_2H_4) and stoichiometric mixture fraction (for both coflow compositions). For Re_{jet}=10,000 the bulk jet exit velocity (U_{jet}) is also shown.

Coflow	C_2H_4	C_2H_4/H_2	C_2H_4/air	C_2H_4/N_2
3% O_2	Attached	Attached	Attached	Attached
9% O_2	26mm	Attached	33mm	34mm

Table 2
Apparent lift-off height estimates based on visual observations for Re_{jet}=10,000.

Species	Coflow	C_2H_4	C_2H_4/H_2	C_2H_4/Air	C_2H_4/N_2
OH	3% O_2	0.14 [27%]	0.64 [10%]	0.17 [41%]	0.15 [30%]
	9% O_2	0.95 [31%]	1.77 [29%]	0.39 [139%]	0.12 [94%]
H_2CO	3% O_2	33 [23%]	14 [28%]	47 [29%]	21 [24%]
	9% O_2	86 [31%]	9 [42%]	56 [35%]	35 [23%]

Table 3
Axial location 35mm above jet exit – Mean and standard deviation (σ, in brackets) of peak OH number density ($\times 10^{16}$cm^{-3}) and peak H_2CO number density (arbitrary units). Re_{jet}=10,000.

Species	Coflow	C_2H_4	C_2H_4/H_2	C_2H_4/Air	C_2H_4/N_2
OH	3% O_2	0.53 [16%]	0.65 [29%]	0.62 [26%]	0.36 [49%]
H_2CO	3% O_2	39 [25%]	12 [44%]	162 [25%]	39 [34%]

Table 4
Axial location 125mm above jet exit – Mean and standard deviation (σ, in brackets) of peak OH number density ($\times 10^{16}$cm^{-3}) and peak H_2CO number density (arbitrary units). Re_{jet}=10,000.

List of Figure Captions

Figure 1: Cross-sectional diagram of JHC burner.

Figure 2: Schematic of experimental layout.

Figure 3: Photographs of ethylene flames for various diluents at Re_{jet}=10,000 for two coflow O_2 levels. Note the different exposure times. Photograph height: 300mm. Horizontal dashed lines indicated measurement locations (35mm & 125mm downstream of jet exit plane).

Figure 4: Apparent lift-off height of 9% O_2 flames at various Reynolds numbers.

Figure 5: Axial location 35mm above jet exit – selection of instantaneous OH, H_2CO and temperature image triplets showing typical features. Re_{jet}=10,000. Each image 8×30mm. Jet centreline marked with dashed line.

Figure 6: H_2CO number density for various fuel compositions from strained laminar flame calculations, in (normalised) mixture fraction space. 3% O_2 coflow oxidant stream, T_{oxi}=1100K. a≈50s^{-1}.

Figure 7: Axial location 35mm above jet exit – selection of instantaneous OH, H_2CO and temperature image triplets showing examples of lifted flames. Re_{jet}=10,000. Each image 8×30mm. Jet centreline marked with dashed line.

Figure 8: Axial location 35mm above jet exit – Mean and RMS radial pro-

files of OH, H_2CO and temperature.

Figure 9: Axial location 125mm above jet exit – Mean and RMS radial profiles of OH, H_2CO and temperature.

Figure 10: Axial location 125mm above jet exit – selection of instantaneous OH, H_2CO and temperature image triplets showing typical features. Re_{jet}=10,000. Each image 8×30mm. Jet centreline marked with dashed line.

Figure 11: Axial location 35mm above jet exit – further selection of instantaneous OH, H_2CO and temperature image triplets. Re_{jet}=10,000. Each image 8×30mm. Jet centreline marked with dashed line.

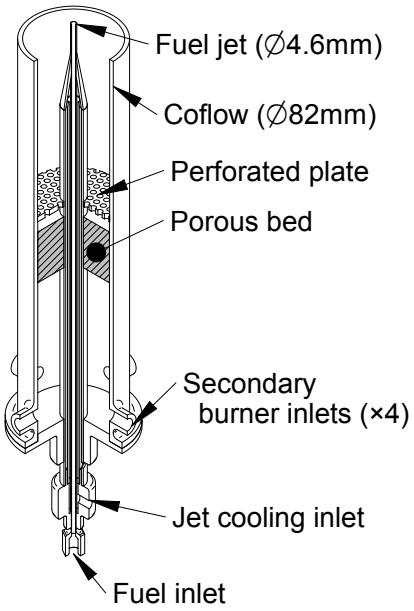

Fig. 1. Cross-sectional diagram of jet in hot coflow (JHC) burner.

Intended figure width=55mm.

C4218 – Medwell, Kalt & Dally.

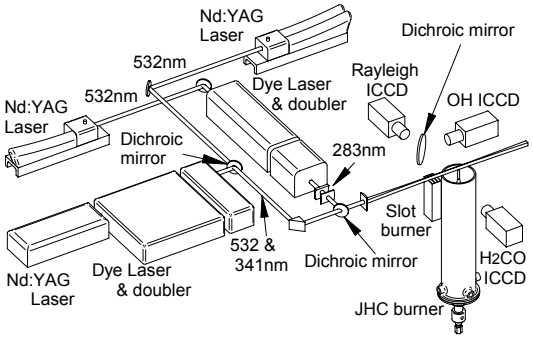

Fig. 2. Schematic of experimental layout.

Intended figure width=70mm.

C4218 – Medwell, Kalt & Dally.

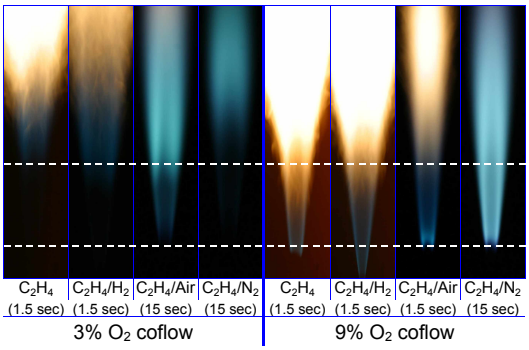

Fig. 3. Photographs of ethylene flames for various diluents at Re_{jet}=10,000 for two coflow O_2 levels. Note the different exposure times. Photograph height: 300mm. Horizontal dashed lines indicated measurement locations (35mm & 125mm downstream of jet exit plane).

Intended figure width=70mm.

C4218 – Medwell, Kalt & Dally.

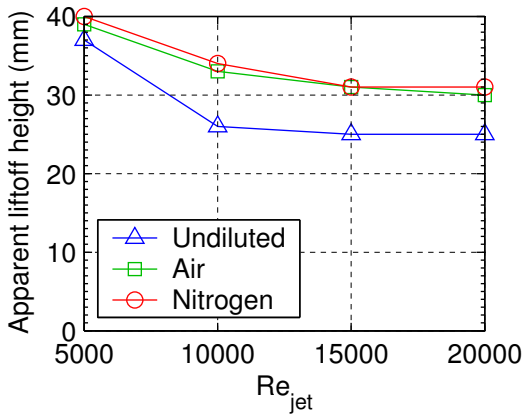

Fig. 4. Apparent lift-off height of 9% O_2 flames at various Reynolds numbers.

Intended figure width=70mm.

C4218 – Medwell, Kalt & Dally.

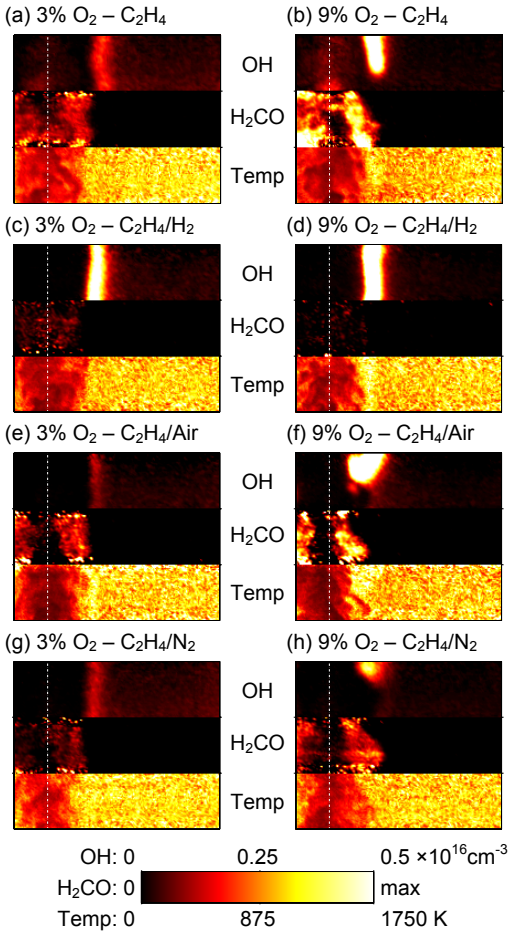

Fig. 5. Axial location 35mm above jet exit – selection of instantaneous OH, H_2CO and temperature image triplets showing typical features. Re_{jet}=10,000. Each image 8×30mm. Jet centreline marked with dashed line.

Intended figure width=70mm.

C4218 – Medwell, Kalt & Dally.

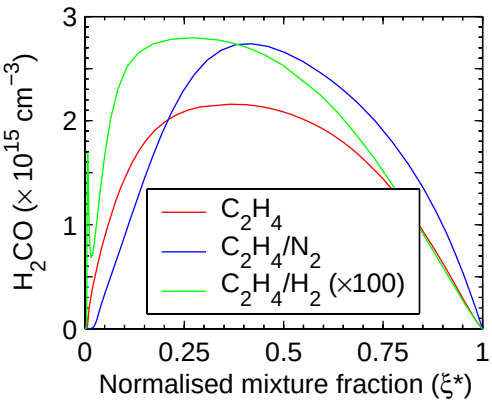

Fig. 6. H_2CO number density for various fuel compositions from strained laminar flame calculations, in (normalised) mixture fraction space. 3% O_2 coflow oxidant stream, T_{oxi}=1100K. a≈50s^{-1}.

Intended figure width=70mm.

C4218 – Medwell, Kalt & Dally.

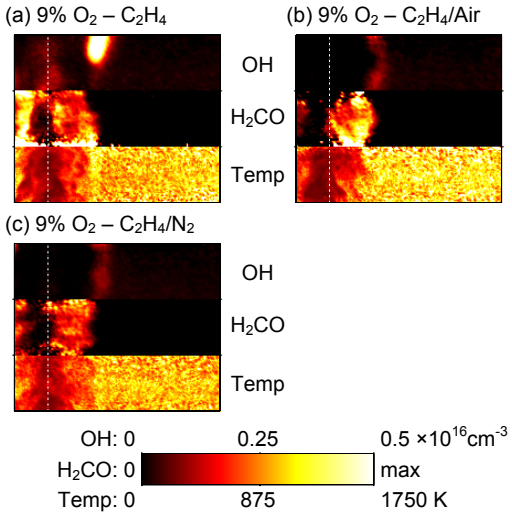

Fig. 7. Axial location 35mm above jet exit – selection of instantaneous OH, H_2CO and temperature image triplets showing examples of lifted flames. Re_{jet}=10,000. Each image 8×30mm. Jet centreline marked with dashed line.

Intended figure width=70mm.

C4218 – Medwell, Kalt & Dally.

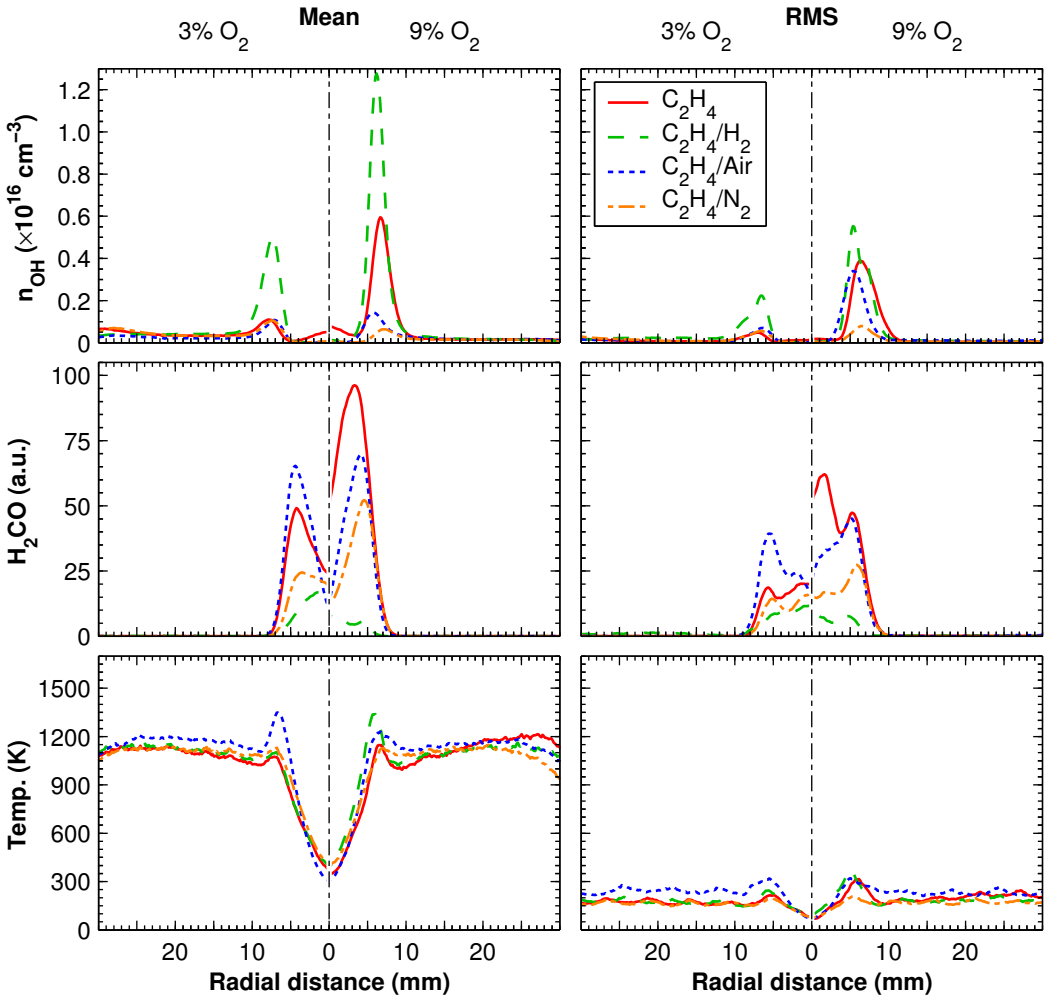

Fig. 8. Axial location 35mm above jet exit – Mean and RMS radial profiles of OH, H_2CO and temperature.

Intended figure width=140mm.

C4218 – Medwell, Kalt & Dally.

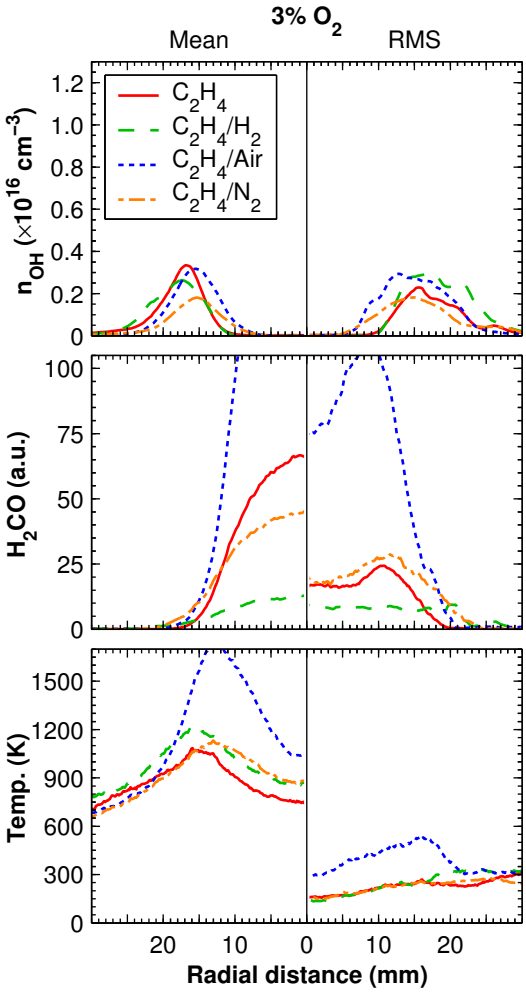

Fig. 9. Axial location 125mm above jet exit – Mean and RMS radial profiles of OH, H_2CO and temperature.

Intended figure width=70mm.
C4218 – Medwell, Kalt & Dally.

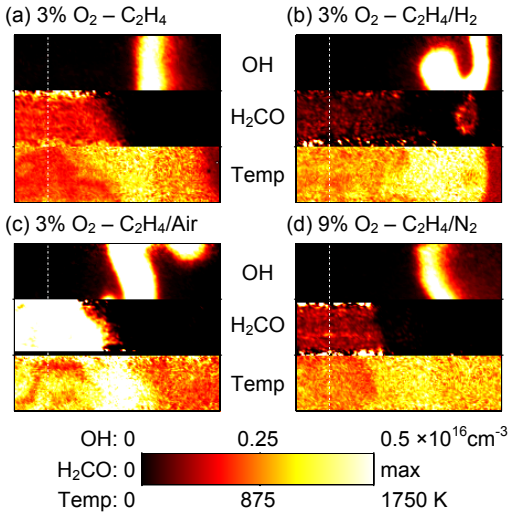

Fig. 10. Axial location 125mm above jet exit – selection of instantaneous OH, H_2CO and temperature image triplets showing typical features. Re_{jet}=10,000. Each image 8×30mm. Jet centreline marked with dashed line.

Intended figure width=70mm.

C4218 – Medwell, Kalt & Dally.

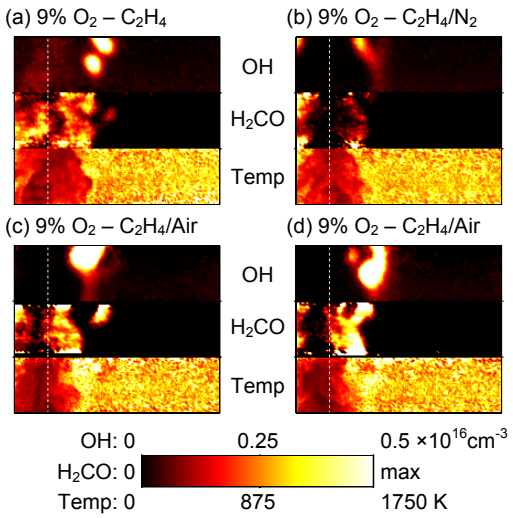

Fig. 11. Axial location 35mm above jet exit – further selection of instantaneous OH, H_2CO and temperature image triplets. Re_{jet}=10,000. Each image 8×30mm. Jet centreline marked with dashed line.

Intended figure width=70mm.

C4218 – Medwell, Kalt & Dally.